ACS OMEGA

Open Access

http://pubs.acs.org/journal/acsodf

Article

Touchless Input/Output Interface for Device-to-Device Communication

Kang Fu, Binju Wang, Jianwei Fu, Jiabin Yan, Pengzhan Liu, and Yongjin Wang*

Cite This: *ACS Omega* 2023, 8, 35336−35342

Read Online

ACCESS | Metrics & More | Article Recommendations

ABSTRACT: Multiple quantum well (MQW) III-nitride diodes show selectable functionalities of light-emitting and light-detecting behaviors, enabling direct touchless device-to-device communication. Here, we propose and demonstrate a touchless input/output (I/O) interface using a single MQW III-nitride diode. By integrating an MQW III-nitride diode with a memory via a control circuit, optical signals are converted into electrical ones to be written into a memory, and consequently, electrical information is read out from the memory to be translated into optical signals for visible light communication (VLC). The MQW III-nitride diode can not only lead to a touchless "writing" action but also offer a "reading" process through light. Such touchless I/O interface would provide new forms of interactivity for device-to-device communication technologies.

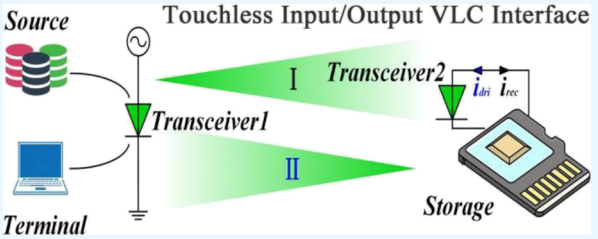

INTRODUCTION

With increasing applications using large datasets, there are higher demands placed on storage methods and storage costs. Especially in interactive interfaces, touchless input/output (I/O) interface is an emerging technology.[1−3] Tang et al.[4] demonstrated the storage of deterministic single photons emitted from a quantum dot in polarization-maintaining solid-state quantum memory. Nakadai et al.[5] reported a photonics−electronics integration solution that realizes the electrical control of a coupled ultrahigh-quality-factor nanocavity system on a silicon chip. Yang et al.[6] realized the storage of photon states in a single nuclear spin. Furthermore, multiple quantum well (MQW) III-nitride diodes are dual-functional devices that provide a new type of solution for this application. Wang et al.[7] proposed a monolithic multicomponent system on a III-nitride-on-silicon platform. Park et al.[8] demonstrated 2000 ppi μLED displays with monolithically integrated thin-film transistor pixel circuits. Farrell et al.[9] realized a hot-carrier-based thermophotonic solar cell. Luo et al.[10] reported a miniaturized optical airflow sensor based on a gallium nitride (GaN) chip with a flexible polydimethylsiloxane (PDMS) membrane. These studies are associated with multifunctional devices that can perform tasks such as energy storage, communication, and sensing. An increasing number of studies are exploring the potential of MQW III-nitride diodes.[11−16] There are few storage interfaces that achieve great function and low cost.[17−19] The development of next-generation memory urgently needs to overcome the constraints of electrical transmission and realize a faster and less interference transmission scheme, and in this regard, the touchless optical I/O interface is a new scheme.[20,21] Oh et al.[22] reported a double heterojunction nanorod device that can be used for simultaneous light emission and detection. Using a dual-functional perovskite diode, Shan et al.[23] proposed a bidirectional optical link between two identical devices. Studies have shown that MQW III-nitride diodes that can not only be used as traditional μLED display lighting but also detect light and modulate light.[24−29] An optical link that uses two identical MQW III-nitride diodes separately acts as the transmitter and the receiver to allow full-duplex communication,[30] and the bandwidth of this transmission mode is sufficient for video transmission.[31] When these diodes are integrated on a large scale, next-generation smart screens can be realized.[32] Studies have shown such designs to exhibit sufficient potential in data communication, but there are few studies on data storage.[33−36] Here, we develop a touchless I/O interface by using the selectable functionalities of the light-emitting and light-detecting behaviors of MQW III-nitride diodes. All data communication is achieved using a single MQW III-nitride diode, and the transmission sequence and rate are soft-defined. This I/O solution offers a cheaper and simpler noncontact channel, which offers value in specific scenarios that require avoiding electromagnetic interference and include higher data security demands. In addition, it mitigates the risks associated with loose or worn contact cables.

Received: July 20, 2023
Accepted: August 30, 2023
Published: September 14, 2023

https://doi.org/10.1021/acsomega.3c05252
ACS Omega 2023, 8, 35336−35342

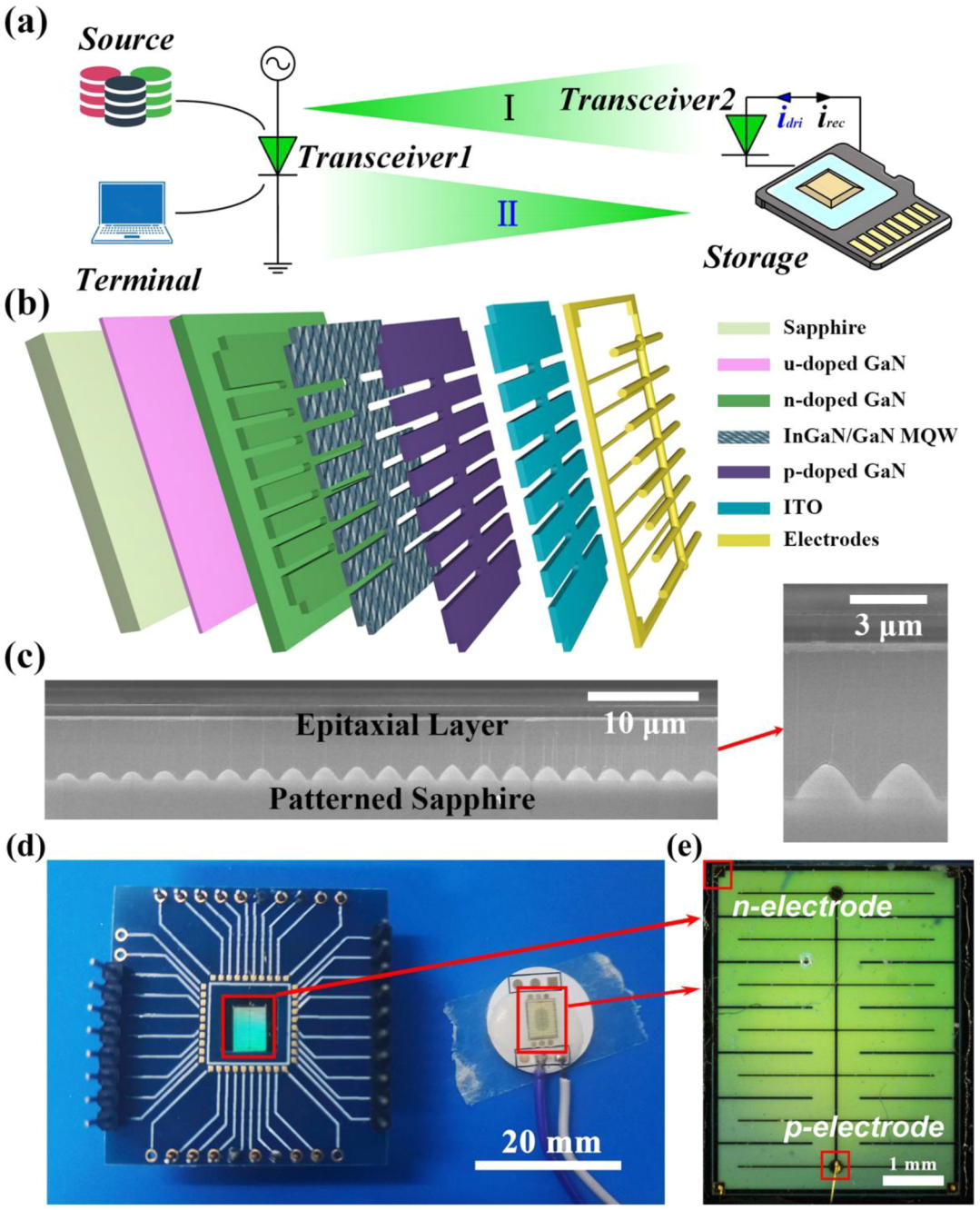

Figure 1. (a) Schematic diagram of the touchless I/O interface; (b) exploded schematic illustration of the MQW III-nitride diode; (c) cross-sectional SEM image of the MQW III-nitride diode; (d) two kinds of circuit packages for MQW III-nitride diodes; (e) optical microscope picture of the MQW III-nitride diode.

DESIGN AND FABRICATION

The touchless I/O interface is schematically illustrated in Figure 1a. Both transceiver1 and transceiver2 are identical MQW III-nitride diodes, which can act as the transmitter and the receiver, respectively. Process I shows a touchless "writing" action. Transceiver1 sends optical signals to be stored, and transceiver2 captures light and converts it into an electrical signal, thereby storing it in the memory. During "reading" process II, data information from memory is encoded into the electrical signals to pulse the light emitted by transceiver2, which is wirelessly transmitted to transceiver1. This directly leads to a touchless "reading" process. Figure 1b shows an exploded schematic illustration of the MQW III-nitride diode.

All MQW III-nitride diodes are manufactured on a commercial 4-inch III-nitride-on-sapphire platform using standard wafer processes from Changelight Co., Ltd. The wafers are also from the company. First, a mesa region is defined by photolithography and inductively coupled plasma (ICP) etching with a depth of 1.4 μm to expose the n-doped GaN surface. Then, the epitaxial film is removed by deep ICP etching, and a 230-nm-thick transparent indium tin oxide (ITO) current spreading layer is deposited by sputtering. After heat treatment, the ITO layer is etched, and Ni/Al/Ti/Pt/Ti/Pt/Au/Ti/Pt/Ti metal stacks are deposited on the n-doped GaN and ITO surfaces. Finally, the sapphire substrate is cleaned and polished down to 200 μm, and the diodes are diced by ultraviolet

https://doi.org/10.1021/acsomega.3c05252
ACS Omega 2023, 8, 35336−35342

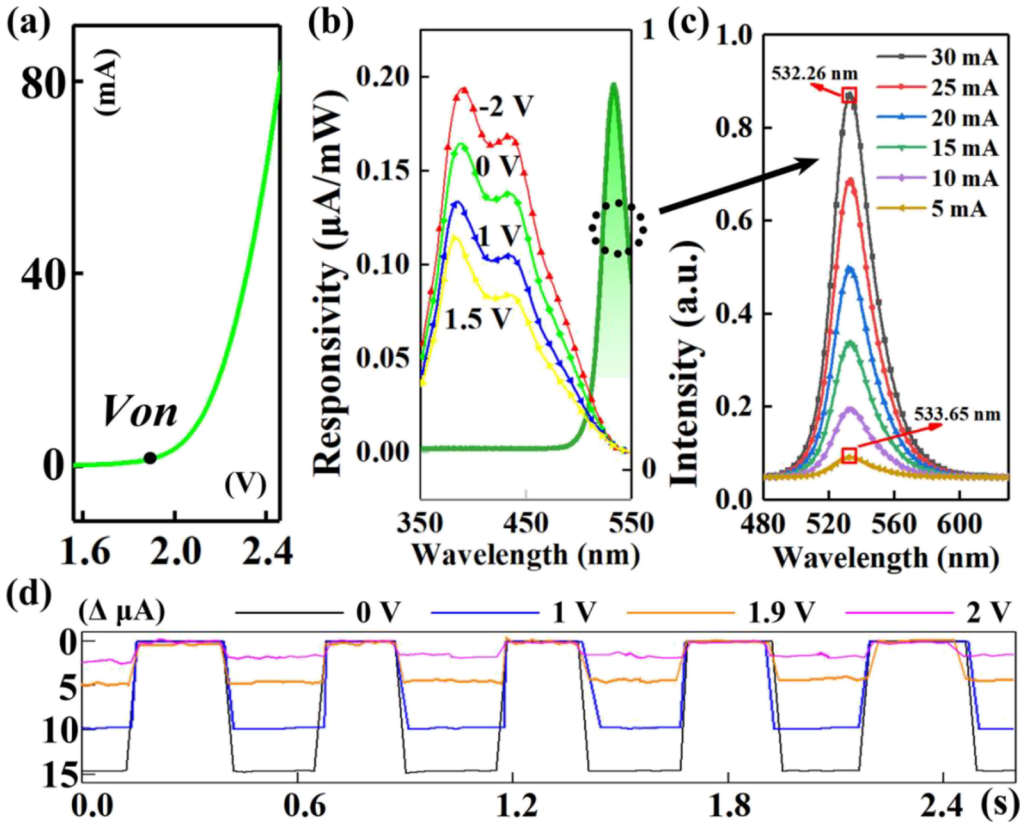

Figure 2. (a) Current−voltage (I−V) curve of the QW diode; (b) detection spectrum of the MQW III-nitride diode; (c) electroluminescence spectrum of the MQW III-nitride diode; (d) circuit-time curve of the MQW III-nitride diode when there are different external excitations.

nanosecond laser micromachining. Figure 1c shows the cross-sectional scanning electron microscope (SEM) image of the MQW III-nitride diode. As shown in Figure 1d, the diode is finally wire-bonded to a printed circuit board (PCB). Figure 1e shows an optical microscope picture of the MQW III-nitride diode. The diode has a thickness of approximately 220 μm, a length of approximately 5.5 mm, a width of approximately 4 mm, and a weight of 105 mg. The four corners of the diode are n-electrodes, from which gold wires are arbitrarily drawn and connected to the PCB to form the ground terminal. In the center of the diode, two p-electrodes are deposited, from which gold wires are drawn and connected to the PCB to form the power supply terminal. We analyze the physical properties of this diode and use it to build a touchless I/O interface.

We characterize the open voltage of the diode by using an Alignet B1500A semiconductor measurement device. Figure 2a shows a typical I−V curve of the diode, which shows that the open voltage of the diode is 1.92 V. When used as a transmitter, we add a voltage of more than 2 V to the MQW III-nitride diode, and when used as a receiver, we ensure that the voltage of the MQW III-nitride diode is below 1.9 V. To ensure the best reception performance of the MQW III-nitride diode when acting as a receiver, we experimentally analyze the selectable functionalities of light-emitting and light-detecting behaviors. When an MQW III-nitride diode acts as a receiver, it can absorb external photons, thereby releasing electron−hole pairs to convert optical signals into electrical signals. We used the OrieliQE-200B measurement device to test the detection spectrum when the bias voltage was −2, 0, 1, and 1.5 V and thus showed that its responsivity decreases with increasing voltage, as shown in Figure 2b. We used the Ocean Optics HR4000 spectrometer to test its electroluminescence spectra, as shown in Figure 2c. When the MQW III-nitride diode is used as a transmitter, as the injection current increases from 5 to 30 mA, the light output of the diode increases so that electricity and information are converted into light and emitted. When the driving current is 5 mA, the main peak is located at 533.65 nm. As the driving current increases to 30 mA, the main peak is slightly skewed to the left, near 532.26 nm. Therefore, combined with Figure 2b,c, we clearly confirm that the emitting spectrum and detection spectrum of this MQW diode have both emission and detection functions within [480, 550 nm].

Therefore, we supply the diode with bias voltages of 0, 1, 1.9, and 2 V, conditions in which the device functions as an optical receiver. Externally, the same diode is used as the transmitter and excited with a frequency of 2 Hz, peak-time value and bias voltage of 2 V to emit light and stimulate the receiver, and the response waveform of the receiver is observed, as shown in Figure 2d. When a bias voltage of 0 V is applied to the receiver, the detection response is the most sensitive, and the photocurrent offset is approximately 15 μA. With increasing voltage, the sensitivity gradually decreases. The diode emits light at a forward voltage of 2 V. At this condition, the diode has a very weak detection ability and its signal is mixed with considerable clutter. At a bias voltage of 2 V, the current variation in its detection signal is merely 2.5 μA. The underlying cause of this phenomenon lies in the intricate balance between the device's light emission and detection processes. Light emission entails a larger direct current component, which consequently makes it more susceptible for the photoelectric current to be "submerged" within the

https://doi.org/10.1021/acsomega.3c05252
ACS Omega 2023, 8, 35336−35342

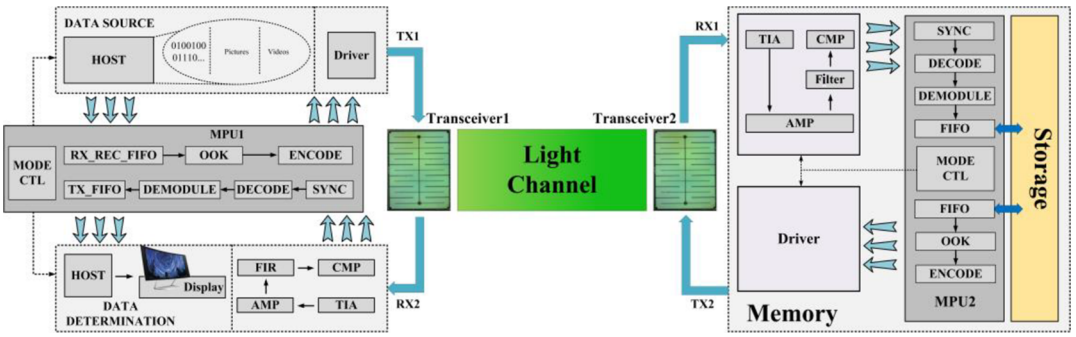

Figure 3. System block diagram of the touchless I/O interface.

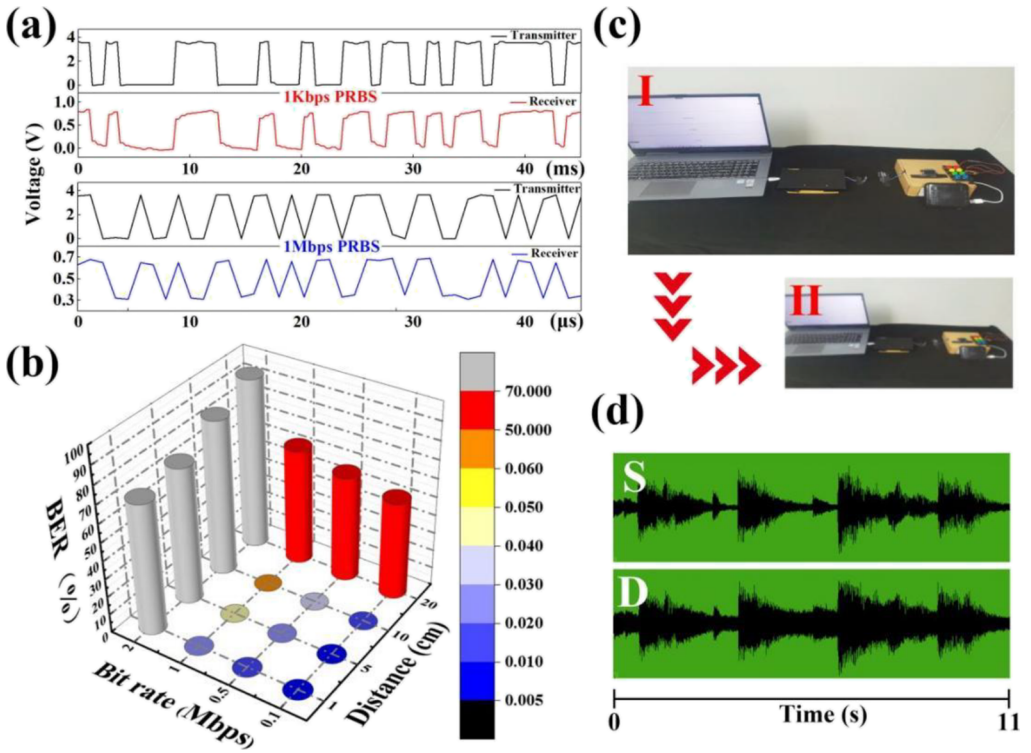

Figure 4. (a) Transmitter−receiver performance of the MQW III-nitride diode at different communication rates; (b) bit error analysis of the MQW III-nitride diode when transmitting bit stream; (c) using the touchless I/O interface to store and read pictures; (d) storage and reading of audio by the touchless I/O interface.

direct current voltage. As depicted in Figure 2b, it is evident that as the applied voltage on the device increases, its detection capability weakens. Therefore, with the amplification of voltage across the device's terminals, the amplitude of the light-generated current change diminishes.

RESULTS AND DISCUSSION

Based on the above testing, the hardware foundation of the touchless I/O interface is established. Combined with certain peripheral circuits and software, the new storage method can be realized. The block diagram of the entire system is shown in Figure 3. This specifically shows a concept of automatic spontaneous adaptive optical I/O. Both "writing" and "reading" processes are realized by using wireless light communication, which leads to a "touchless" I/O interface. When the system works normally, it is divided into a ″writing″ process and a ″reading″ process. In the ″writing″ procedure, the host can send the byte stream, picture or audio data source accordingly, through microprocessor unit cross-clock processing, modulation, encoding, and then it is sent to the driver circuit. The TX1 signal coming from the driver circuit drives transceiver 1 (output) to emit light, and after passing through the spatial channel, it is received by transceiver 2 (input) and then generates the RX1 signal. After transmission amplification, two-stage amplification, filtering, and comparison, the photocurrent is sent to the microprocessor on the storage side for synchronization, decoding, demodulation, and storage. During the reading process, the microprocessor at the storage side modulated and coded the stored data and drove the TX2 signal from transceiver2 (output) to emit light through the driver circuit. After passing through the spatial channel, transceiver1 (input) acts as the receiver to receive data and generate the RX2 signal. After undergoing the same receiving process as described above, the data are restored and displayed in the terminal host. Our touchless optical I/O interface has various potential application scenarios. For example, a touchless shared user terminal that communicates with each other via light is highly required to eliminate the need for

https://doi.org/10.1021/acsomega.3c05252
ACS Omega 2023, 8, 35336−35342

manual operation to reduce the risk of cross-contamination due to contact with handwritten terminals.

Figure 4a shows the communication waveform of a pair of MQW III-nitride diodes at communication rates of 1 kbps and 1 Mbps. A key requirement for faster communication is to decrease the device size. Smaller diodes can be modulated faster and have lower power consumption; however, their communication distance is limited. We can achieve a higher response bandwidth by reducing the size and thickness of the diode, thereby reducing the RC time constant of the diode. The waveform spikes after the speed increases, but the demodulation condition is still satisfied after the comparator and other circuits are finished processing. To enrich the test data of the byte stream transmission, we test its bit error rate (BER) at different distances and different transmission rates, send the data stream of 100,000 bits every 20 times, and calculate the average BER, which is calculated according to eq 1. The results are shown in Figure 4b. It is evident that at a bit rate of 0.1 Mbps and a distance of 10 cm, the BER remains below 0.01%. Similarly, at a bit rate of 0.5 Mbps and the same distance, the BER remains below 0.04%, increasing as the distance grows. As the bit rate is further increased to 1 Mbps, the BER rises to 0.06%. These levels of BER are acceptable for signal transmission. However, at a bit rate of 2 Mbps or a distance of 20 cm, the BER sharply increases, rendering the signal unable to be accurately transmitted. The system can achieve low BER under the condition of satisfying a certain distance and a certain rate, which are related to the transmission power, transmission distance, receiving cutoff bandwidth of the device, and quantum efficiency of the device. Equation 1 is given as follows:

$$\mathrm{BER} = \frac{N_e}{N_s} = \frac{N_{e(tx)} + N_{e(rx)}}{N_s} \quad (1)$$

where N_e is the total number of error bits, N_s is the total number of sent bits, $N_{e(tx)}$ is the total number of error bits in the storage process, and $N_{e(rx)}$ is the total number of error bits in the reading process.

Figure 4c illustrates the results of storing pictures by the touchless storage system: selecting our test photos as the test images to be stored, the original pictures are I, and the restored pictures are II. The data show that the pictures are correctly restored. Although some white noise is introduced through the spatial channel, certain image processing means can be added in the later stage to fully restore the image. Figure 4d shows the storage of an 11-second audio file, where S is the source voice waveform and D is the destination voice waveform. The results show that audio can also be stored and restored in this fashion. We conducted system testing under different environmental conditions, and the optimal operating temperature of the system primarily depends on the diode chip. The optimal range is approximately −20 to 65 °C and the overall system power is approximately 1.5 W. Throughout the 72 h testing period, the system's communication remained stable.

Compared to other existing I/O interface technologies, optical communication interfaces exhibit irreplaceability in specific application scenarios. These include environments with stringent electromagnetic interference requirements, hazardous areas with flammable materials or chemicals, situations demanding wireless communication, and cases requiring area isolation. The detailed comparisons are presented in Table 1.

Table 1. Compared with Existing I/O Interface Technologies

I/O interface	USB	ethernet	bluetooth	VLC
high data rate/reliability	○	○		
strong EMI resistance				○
noncontact operation			○	○
low power consumption	○	○	○	○

While optical communication inherently possesses strong resistance to electromagnetic interference, how to ensure the system's immunity to electromagnetic interference (EMI) remains a critical consideration. We can employ the following means to shield against electromagnetic interference as effectively as possible: (a) directional fixture of MQW diode: ensuring a fixed orientation for the MQW diode, which allows light signals to transmit only in the intended direction, thereby reducing electromagnetic interference from other directions. (b) Internal filters: integrating filters within the device to minimize the ingress of external electromagnetic signals. (c) Effective signal processing and error correction coding: implementing robust signal processing and error correction coding to enhance the system's immunity to interference. (d) Structural design considerations: incorporating shielding measures into the structural design, including well-placed ground connections and electromagnetic shielding structures. (e) Additional measures: these include selecting shielding materials, positioning the device away from sources of interference, and implementing optical isolation during light communication. The implementation of these measures should be tailored to the specific requirements of the system setup.

CONCLUSIONS

In summary, the selectable functionalities of MQW III-nitride diodes enable new forms of information and energy conversion between photons and electrons, allowing one device to transmit and receive information at the same time. By integrating with programmed circuits, MQW III-nitride diodes introduce new feasible routes toward touchless I/O interfaces. The user terminals communicate with each other via light and thus provide noncontact reader/writer interfaces. We therefore intend that multifunctional III-nitride technology will contribute to the upcoming proliferation of Internet of Things applications.

ASSOCIATED CONTENT

Data Availability Statement

The authors confirm that the data supporting the findings of this study are available within the article.

AUTHOR INFORMATION

Corresponding Author

Yongjin Wang − *GaN Optoelectronic Integration International Cooperation Joint Laboratory of Jiangsu Province, Nanjing University of Posts and Telecommunications, Nanjing 210003, China;* orcid.org/0000-0001-8109-4640; Email: wangyj@njupt.edu.cn

Authors

Kang Fu − *GaN Optoelectronic Integration International Cooperation Joint Laboratory of Jiangsu Province, Nanjing University of Posts and Telecommunications, Nanjing 210003, China;* orcid.org/0000-0003-1239-7685

https://doi.org/10.1021/acsomega.3c05252
ACS Omega 2023, 8, 35336−35342

Binju Wang − *GaN Optoelectronic Integration International Cooperation Joint Laboratory of Jiangsu Province, Nanjing University of Posts and Telecommunications, Nanjing 210003, China*

Jianwei Fu − *GaN Optoelectronic Integration International Cooperation Joint Laboratory of Jiangsu Province, Nanjing University of Posts and Telecommunications, Nanjing 210003, China*

Jiabin Yan − *GaN Optoelectronic Integration International Cooperation Joint Laboratory of Jiangsu Province, Nanjing University of Posts and Telecommunications, Nanjing 210003, China;* orcid.org/0000-0003-2460-5832

Pengzhan Liu − *GaN Optoelectronic Integration International Cooperation Joint Laboratory of Jiangsu Province, Nanjing University of Posts and Telecommunications, Nanjing 210003, China*

Complete contact information is available at: https://pubs.acs.org/10.1021/acsomega.3c05252

Author Contributions

Y.W. conceived and designed the experiments, performed the experiments, analyzed the data, contributed materials and analysis tools, and wrote the paper. K.F., B.W., J.F., J.Y., X.J., and P.L. performed the experiments. K.F. analyzed the data and drafted the paper. K.F. and B.W. contributed equally to the article. All authors reviewed the manuscript.

Notes

The authors declare no competing financial interest.

■ ACKNOWLEDGMENTS

This work was jointly supported by the National Key Research and Development Program of China (2022YFE0112000), 111 Project (D17018), and National Natural Science Foundation of China (61827804, U21A201550), and Jiangsu Province Innovation Plan Project (KYCX22_0935).

■ REFERENCES

(1) Wang, Y.; Li, J.; Zhang, S.; Su, K.; Zhou, Y.; Liao, K.; Du, S.; Yan, H.; Zhu, S.-L. Efficient quantum memory for single-photon polarization qubits. *Nat. Photonics* **2019**, *13*, 346−351.

(2) Distante, E.; Farrera, P.; Padrón-Brito, A.; Paredes-Barato, D.; Heinze, G.; Riedmatten, H. D. Storing single photons emitted by a quantum memory on a highly excited Rydberg state. *Nat. Commun.* **2017**, *8*, 14072.

(3) Yanik, M. F.; Fan, S. Dynamic photon storage. *Nat. Phys.* **2007**, *3*, 372−374.

(4) Tang, J.-S.; Zhou, Z.-Q.; Wang, Y.-T.; Li, Y.-L.; Liu, X.; Hua, Y.-L.; Zou, Y.; Wang, S.; He, D.-Y.; Chen, G.; Sun, Y.-N.; Yu, Y.; Li, M.-F.; Zha, G.-W.; Ni, H.-Q.; Niu, Z.-C.; Li, C.-F.; Guo, G.-C. Storage of multiple single-photon pulses emitted from a quantum dot in a solid-state quantum memory. *Nat. Commun.* **2015**, *6*, 8652.

(5) Nakadai, M.; Asano, T.; Noda, S. Electrically controlled on-demand photon transfer between high-Q photonic crystal nano-cavities on a silicon chip. *Nat. Photonics* **2022**, *16*, 113−118.

(6) Yang, S.; Wang, Y.; Rao, D. D. B.; Tran, T. H.; Momenzadeh, A. S.; Markham, M.; Twitchen, D. J.; Wang, P.; Yang, W.; Stöhr, R.; Neumann, P.; Kosaka, H.; Wrachtrup, J. High-fidelity transfer and storage of photon states in a single nuclear spin. *Nat. Photonics* **2016**, *10*, 507−511.

(7) Wang, Y.; Wang, X.; Zhu, B.; Shi, Z.; Yuan, J.; Gao, X.; Liu, Y.; Sun, X.; Li, D.; Amano, H. Full-duplex light communication with a monolithic multicomponent system. *Light Sci.: Appl.* **2018**, *7*, 83.

(8) Park, J.; Choi, J. H.; Kong, K.; Han, J. H.; Park, J. H.; Kim, N.; Lee, E.; Kim, D.; Kim, J.; Chung, D.; Jun, S.; Kim, M.; Yoon, E.; Shin, J.; Hwang, S. Electrically driven mid-submicrometre pixelation of InGaN micro-light-emitting diode displays for augmented-reality glasses. *Nat. Photonics* **2021**, *15*, 449−455.

(9) Farrell, D. J.; Sodabanlu, H.; Wang, Y.; Sugiyama, M.; Okada, Y. A hot-electron thermophotonic solar cell demonstrated by thermal up-conversion of sub-bandgap photons. *Nat. Commun.* **2015**, *6*, 8685.

(10) Luo, Y.; An, X.; Chen, L.; Li, K. H. Chip-scale optical airflow sensor. *Microsyst. Nanoeng.* **2022**, *8*, 4.

(11) Li, X.; Wang, Y.; Hane, K.; Shi, Z.; Yan, J. GaN-based integrated photonics chip with suspended LED and waveguide. *Opt. Commun.* **2018**, *415*, 43−47.

(12) Nargelas, S.; Mickevičius, J.; Kadys, A.; Jarašiūnas, K.; Malinauskas, T. Stimulated emission threshold in thick GaN epilayers: interplay between charge carrier and photon dynamics. *Opt. Laser Technol.* **2021**, *134*, No. 106624.

(13) Feng, M.; Wang, J.; Zhou, R.; Sun, Q.; Gao, H.; Zhou, Y.; Liu, J.; Huang, Y.; Zhang, S.; Ikeda, M.; Wang, H.; Zhang, Y.; Wang, Y.; Yang, H. On-chip integration of GaN-based laser, modulator, and photodetector grown on Si. *IEEE J. Sel. Top. Quantum Electron.* **2018**, *24*, 1−5.

(14) Bao, C.; Xu, W.; Yang, J.; Bai, S.; Teng, P.; Yang, Y.; Wang, J.; Zhao, N.; Zhang, W.; Huang, W.; Gao, F. Bidirectional optical signal transmission between two identical devices using perovskite diodes. *Nat. Electron.* **2020**, *3*, 156−164.

(15) Li, Z.; Waldron, J.; Detchprohm, T.; Wetzel, C.; Karlicek, R. F.; Chow, T. P. Monolithic integration of light-emitting diodes and power metal-oxide-semiconductor channel high-electron-mobility transistors for light-emitting power integrated circuits in GaN on sapphire substrate. *Appl. Phys. Lett.* **2013**, *102*, No. 192107.

(16) Heo, S. Y.; Kim, J.; Gutruf, P.; Banks, A.; Wei, P.; Pielak, R.; Balooch, G.; Shi, Y.; Araki, H.; Rollo, D.; Gaede, C.; Patel, M.; Kwak, J. W.; Peña-Alcántara, A. E.; Lee, K.-T.; Yun, Y.; Robinson, J. K.; Xu, S.; Rogers, J. A. Wireless, battery-free, flexible, miniaturized dosimeters monitor exposure to solar radiation and to light for phototherapy. *Sci. Transl. Med.* **2018**, *10*, No. eaau1643.

(17) Wang, T.; Meng, J.; Zhou, X.; Liu, Y.; He, Z.; Han, Q.; Li, Q.; Yu, J.; Li, Z.; Liu, Y.; Zhu, H.; Sun, Q.; Zhang, D. W.; Chen, P.; Peng, H.; Chen, L. Reconfigurable neuromorphic memristor network for ultralow-power smart textile electronics. *Nat. Commun.* **2022**, *13*, 7432.

(18) Pan, C.; Tabatabaei, S. K.; Yazdi, S. M. H. T.; Hernandez, A. G.; Schroeder, C. M.; Milenkovic, O. Rewritable two-dimensional DNA-based data storage with machine learning reconstruction. *Nat. Commun.* **2022**, *13*, 2984.

(19) Dashtdar, M.; Flah, A.; Hosseinimoghadam, S. M. S.; El-Fergany, A. Frequency control of the islanded microgrid including energy storage using soft computing. *Sci. Rep.* **2022**, *12*, 20409.

(20) Li, J.; Ye, D.; Fu, K.; Wang, L.; Piao, J.; Wang, Y. Single-photon detection for MIMO underwater wireless optical communication enabled by arrayed LEDs and SiPMs. *Opt. Express* **2021**, *29*, 25922.

(21) Hardtdegen, H.; Mikulics, M. Towards III-nitride nano-LED based single photon emitters: technology and applications. In *2016 11th International Conference on Advanced Semiconductor Devices & Microsystems (ASDAM)*, 2016; pp 27−32.

(22) Oh, N.; Kim, B. H.; Cho, S.-Y.; Nam, S.; Rogers, S. P.; Jiang, Y.; Flanagan, J. C.; Zhai, Y.; Kim, J.-H.; Lee, J.; Yu, Y.; Cho, Y. K.; Hur, G.; Zhang, J.; Trefonas, P.; Rogers, J. A.; Shim, M. Double-heterojunction nanorod light-responsive LEDs for display applications. *Science* **2017**, *355*, 616−619.

(23) Shan, Q.; Wei, C.; Jiang, Y.; Song, J.; Zou, Y.; Xu, L.; Fang, T.; Wang, T.; Dong, Y.; Liu, J.; Han, B.; Zhang, F.; Chen, J.; Wang, Y.; Zeng, H. Perovskite light-emitting/detecting bifunctional fibres for wearable LiFi communication. *Light Sci.: Appl.* **2020**, *9*, 163.

(24) Shi, Z.; Yuan, J.; Zhang, S.; Liu, Y.; Wang, Y. Simultaneous dual-functioning InGaN/GaN multiple-quantum-well diode for transferrable optoelectronics. *Opt. Mater.* **2017**, *72*, 20−24.

(25) Wang, Y.; Xu, Y.; Yang, Y.; Gao, X.; Zhu, B.; Cai, W.; Yuan, J.; Zhang, R.; Zhu, H. Simultaneous light emission and detection of InGaN/GaN multiple quantum well diodes for in-plane visible light communication. *Opt. Commun.* **2017**, *387*, 440−445.

(26) Wang, Y.; Zhu, G.; Cai, W.; Gao, X.; Yang, Y.; Yuan, J.; Shi, Z.; Zhu, H. On-chip photonic system using suspended p-n junction InGaN/GaN multiple quantum wells device and multiple waveguides. *Appl. Phys. Lett.* **2016**, *108*, No. 162102.
(27) Sakowicz, M.; Sai, P.; But, D. B.; Cywinski, G.; Dub, M.; Kasalynas, I.; Prystawko, P.; Rumyantsev, S.; Knap, W. AlGaN/GaN HEMTs for THz plasma wave detection and emission. In *2020 45th International Conference on Infrared, Millimeter, and Terahertz Waves (IRMMW-THz)*, 2020; pp 1−2.
(28) Wang, Y.; Wang, S.; Ni, S.; Wang, W.; Shi, Z.; Yuan, J.; Zhu, H. On-chip multicomponent system made with vertical structure quantum well diode. *Semicond. Sci. Technol.* **2019**, *34*, No. 065017.
(29) Gao, X.; Shi, Z.; Zhu, B.; Wu, F.; Yuan, J.; Qin, C.; Jiang, Y.; Cai, W.; Wang, Y. Tandem dual-functioning multiple-quantum-well diodes for a self-powered light source. *Opt. Lett.* **2018**, *43*, 3710−3713.
(30) Fu, K.; Gao, X.; Yin, Q.; Yan, J.; Ji, X.; Wang, Y. Full-duplex visible light communication system using a single channel. *Opt. Lett.* **2022**, *47*, 4802−4805.
(31) Fu, K.; Gao, X.; Ye, Z.; Li, J.; Ji, X.; Wang, Y. Coexistence of light emission and detection in a III-nitride quantum well diode. *Opt. Lett.* **2022**, *47*, 2614.
(32) Fu, K.; Gao, X.; Qin, F.; Song, Y.; Wang, L.; Ye, Z.; Su, Y.; Zhu, H.; Ji, X.; Wang, Y. Simultaneous Illumination-Imaging. *Adv. Mater. Technol.* **2021**, *6*, No. 2100227.
(33) Li, J.; Wu, J.; Chen, L.; An, X.; Yin, J.; Wu, Y.; Zhu, L.; Yi, H.; Li, K. H. On-chip integration of III-nitride flip-chip light-emitting diodes with photodetectors. *J. Light. Technol.* **2021**, *39*, 2603−2608.
(34) Ren, A.; Wang, H.; Zhang, W.; Wu, J.; Wang, Z.; Penty, R. V.; White, I. H. Emerging light-emitting diodes for next-generation data communications. *Nat. Electron.* **2021**, *4*, 559−572.
(35) Wang, Q.; Yuan, G.-D.; Liu, W.-Q.; Zhao, S.; Zhang, L.; Liu, Z.-Q.; Wang, J.-X.; Li, J.-M. Monolithic semi-polar (1101) InGaN/GaN near white light-emitting diodes on micro-striped Si (100) substrate. *Chin. Phys. B* **2019**, *28*, No. 087802.
(36) Mikulics, M.; Kordoš, P.; Gregušová, D.; Sofer, Z.; Winden, A.; Trellenkamp, S.; Moers, J.; Mayer, J.; Hardtdegen, H. Conditioning nano-LEDs in arrays by laser-micro-annealing: the key to their performance improvement. *Appl. Phys. Lett.* **2021**, *118*, No. 043101.

https://doi.org/10.1021/acsomega.3c05252
ACS Omega 2023, 8, 35336−35342